http://dx.doi.org/10.5516/NET.09.2011.072

# STRUCTURAL TEST AND ANALYSIS OF RC SLAB AFTER FIRE LOADING

CHUL-HUN CHUNG[1], CHO RONG IM[2], and JAEGYUN PARK[3*]
[1]Professor, Dept. of Civil & Environmental Engineering, Dankook University
Yong-In, Korea
[2]Graduate Student, Dept. of Civil & Environmental Engineering, Dankook University
Yong-In, Korea
[3]Associate Professor, Dept. of Civil & Environmental Engineering, Dankook University
Yong-In, Korea
[*]Corresponding author. E-mail : jpark@dankook.ac.kr

*Received December 05, 2011*
*Accepted for Publication July 24, 2012*

In the present study the behavior of fire and the residual strength of fire-ignited RC slabs are investigated by experimental tests and numerical simulations. The fire tests of RC slabs were carried out in a furnace using the ISO 834 standard fire. The load capacity of the cooled RC slabs that were not loaded during the fire tests was evaluated by additional 3 point bending tests. The influence of the proportion of PP (polypropylene) fibers in the RC slabs on the structural behavior of the RC slabs after the fire loading was investigated. The results of the fire tests showed that the maximum temperature of concrete with PP fiber was lower than that of concrete without PP fiber. As the concrete was heated, the ultimate compressive strength decreased and the ultimate strain increased. The load-deflection relations of RC slabs after fire loading were compared by using existing stress-strain-temperature models. The comparison between the numerical analysis and the experimental tests showed that some numerical analyses were reliable and therefore, can be applied to evaluate the ultimate load of RC slabs after fire loading. The ultimate load capacity after cooling down the RC slabs without PP fiber showed a considerable reduction from that of the RC slabs with PP fiber.

**KEYWORDS** : ISO 834 Standard Fire, Concrete with PP (Polypropylene) Fiber, Stress-strain-temperature Model, Ultimate Load after Fire Loading, Numerical Analysis

## 1. INTRODUCTION

Concrete has superior fire resistance among structural materials, but its behavior under high temperature conditions is quite different from that under general conditions. The temperature of a very thick RC structure generally does not increase globally due to its low thermal conductivity, therefore it is considered as a fire resistant structure. However, the surface of concrete exposed to a high temperature fire can be torn off by explosive spalling. Studies have been done on the prevention of concrete spalling and temperature increase of the steel embedded in the concrete [1, 2, 3, 4, and 5]. Kim et al [6] applied a fiber cocktail, which consists of PP and steel fiber, to concrete and evaluated the thermal characteristics of the fiber cocktail embedded concrete including compressive strength, elastic modulus and specific heat.

The stress-strain curve of a concrete structure is greatly affected by thermal loading. To evaluate the resistance of a structure right after thermal damage, a material model with proper thermal parameters must be chosen. Lie [7] proposed a stress-strain relation that considered the temperature effect based on the model by Ritter [8] and Hognestad [9]. Schneider suggested another stress-strain curve that considered the temperature parameter, which referred to EUROCODE 2 [10]. Shi et al [11] made a model whose loading curve was different from the unloading curve under thermal load. Nan et al [12] proposed a model, whose behavior was consistent up to 300ºC and the strength decreased with increasing maximum strain for temperatures over 300ºC EUROCODE 2 [10] specified a model, which was divided by an initial curved line of hardening, followed by a straight line of softening. The stress-strain curve of a steel member is strongly affected by thermal load, but it recovers its original shape after the member cools down [13].

In this study, one ordinary specimen and one fire resistant specimen with 0.1% PP fiber (Fig. 1) were assumed to be simply supported and tested according to ISO 834 (Fig. 2), and the temperature was measured at several depths of the concrete slab. After the thermal loading test, the resistance of the cooled down structure was evaluated. Related to this study, the performance of an undamaged

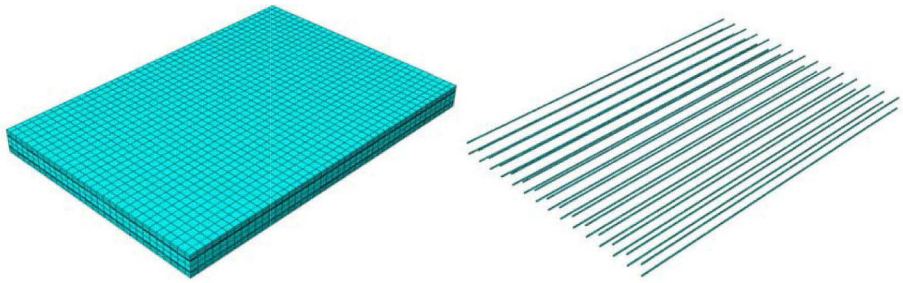

(a) Model of the concrete slab (b) model of the rebar

Fig. 1. Shape of the Specimen

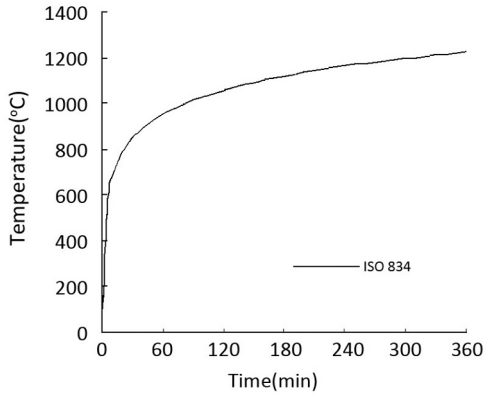


Fig. 2. ISO-834 Fire Curve

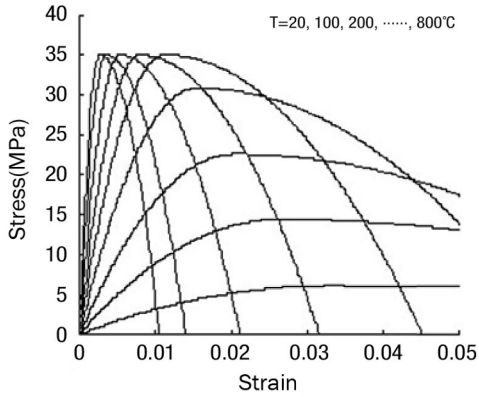


Fig. 3. Lie's Concrete Model [7]

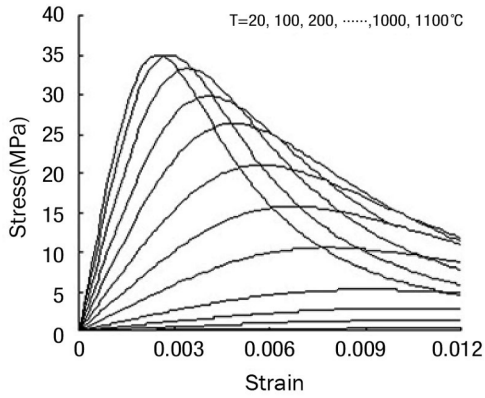


Fig. 4. Schneider's Concrete Model [15]

concrete slab was evaluated by C.-H. Chung et al [22]. The stress-strain relations of existing studies were reviewed and calibrated using the recorded temperature at each depth. These stress-strain relations were selected for nonlinear finite element analysis. The effect of thermal loading was best described by a specific material model and this finding is one of the main purposes of this study.

## 2. STRESS-STRAIN RELATIONS UNDER THERMAL LOADING

### 2.1 Concrete Model

Lie [7] suggested stress-strain relations (1)-(3) considering the temperature effect based on the stress-strain curve proposed by Ritter [8] and Hognestad [9]. This model is well presented in Fig. 3, in which the result of Schneider and Haksever [14] is included and the creep at high temperature is considered.

$$f_c = \begin{cases} f_c' \left[1 - \left(\frac{\varepsilon_{max} - \varepsilon_c}{\varepsilon_{max}}\right)^2\right] & : \ \varepsilon_c \le \varepsilon_{max} \\ f_c' \left[1 - \left(\frac{\varepsilon_c - \varepsilon_{max}}{3\varepsilon_{max}}\right)^2\right] & : \ \varepsilon_c > \varepsilon_{max} \end{cases} \quad (1)$$

$$f_c' = \begin{cases} f_{co}' & : \ T < 450\,℃ \\ f_{co}' \left[2.011 - 2.353\frac{T-20}{1000}\right] & : \ T \ge 450\,℃ \end{cases} \quad (2)$$

$$\varepsilon_{max} = 0.0025 + (6.0T + 0.04T^2) \times 10^{-6} \quad (3)$$

$f_c$ : strength of concrete at T°C(MPa)
$f_c'$ : strength of cylinder concrete at T°C(MPa)
$f_{co}'$ : strength of cylinder concrete at room temperature (MPa)
$\varepsilon_c$ : strain of concrete at temperature 20°C
$\varepsilon_{max}$ : strain of concrete at the maximum stress

Schneider [15] suggested a temperature dependent stress-strain curve, as given by eq. (4), where the maximum strain $\varepsilon_{c1,T}$ is calculated by eq. (5) of Franssen [16]. In eqs. (4) and (5), a temperature increase leads to both a decrease

of $f_{c,T}$ and an increase of $\varepsilon_{cu,T}$, where the reduction coefficient in table 1 based on EUROCODE 2 [10] is used.

$$\frac{f}{f_{c,T}} = \frac{n(\varepsilon_\sigma/\varepsilon_{c1,T})}{(n-1)+(\varepsilon_\sigma/\varepsilon_{c1,T})^n} \qquad \varepsilon_\sigma \le \varepsilon_{cu,T} \tag{4}$$

$$\varepsilon_{c1,T} = 2.5\times10^{-3} + 4.1\times10^{-6}(T-20) + 5.5\times10^{-9}(T-20)^2 \le 10^{-3} \tag{5}$$

$\varepsilon_{c1,T}$ : strain value corresponding to compressive strength $f_{c,T}$ at temperature TºC.
$f_{c,T}$ : compressive strength of concrete at temperature TºC(MPa)
$\varepsilon_{cu,T}$ : ultimate strain at temperature TºC
$n$ : 3
$f_c$ : compressive strength of concrete at T=20ºC (MPa)

The compressive strength of concrete $f_c^T$ is constant up to the temperature of 200ºC. When the temperature exceeds 200ºC, the compressive strength of concrete decreases generally and is 15% of the original strength at 800ºC. From these observations, Shi et al [11] presented the relation between $f_c^T$ and T in eq. (6). The strain of concrete at the maximum stress, $\varepsilon_{\sigma o}$, increases rapidly as the temperature increases, which is described in eq.(8).

$$f_c{}^T = \frac{f_c}{1+14.5\gamma^{4.2}} \qquad 20\,℃ \le T \le 800\,℃ \tag{6}$$

$$\gamma = (T-20)/1{,}000 \tag{7}$$

$$\varepsilon_{\sigma o} = (1-1.55\gamma+8.27\gamma^2)\varepsilon_o \quad 20\,℃ \le T \le 800\,℃ \tag{8}$$

$\varepsilon_o$ : strain corresponding to $f_c$ at room temperature

**Table 1**. Compressive Strength Ratio, $f_{c,t}/f_c$, $\varepsilon_{c1,T}$ and $\varepsilon_{cu,T}$ [10]

| Temperature (°C) | $f_{c,t}/f_c$ | $\varepsilon_{c1,T}$ | $\varepsilon_{cu,T}$ |
|---|---|---|---|
| 20 | 1.0 | 0.0025 | 0.0200 |
| 100 | 0.95 | 0.0040 | 0.0225 |
| 200 | 0.90 | 0.0055 | 0.0250 |
| 300 | 0.85 | 0.0070 | 0.0275 |
| 400 | 0.75 | 0.0100 | 0.0300 |
| 500 | 0.60 | 0.0150 | 0.0325 |
| 600 | 0.45 | 0.0250 | 0.0350 |
| 700 | 0.30 | 0.0250 | 0.0375 |
| 800 | 0.15 | 0.0250 | 0.0400 |
| 900 | 0.08 | 0.0250 | 0.0425 |
| 1000 | 0.04 | 0.0250 | 0.0450 |
| 1100 | 0.01 | 0.0250 | 0.0475 |
| 1200 | 0.0 | - | - |

$\varepsilon_{\sigma o}$ : strain corresponding to $f_c^T$ at temperature TºC

A temperature increase leads to both the decrease of $f_c^T$ and the increase of $\varepsilon_{\sigma o}$ such that the slope of the increasing part of the curve is decreased. The decreasing part of the stress-strain curve is different from the increasing part because the decrease of the stress occurs more slowly at a high temperature than at a low temperature. According to this result, Shi et al [11] suggested another temperature dependent stress-strain curve in eq. (9) and the shape of this model is presented in Fig. 5.

$$y = 2x - x^2 (0 \le x \le 1) \tag{9a}$$

$$y = \frac{x}{2(x-1)^2+x} (x > 1) \tag{9b}$$

$$y = f/f_c{}^T \tag{9c}$$

$$x = \varepsilon_\sigma/\varepsilon_{\sigma o} \tag{9d}$$

$f$ : stress of concrete (MPa)

Fig. 6 presents another model by Nan et al [12], where the compressive strength of concrete decreases and the corresponding maximum strain increases above a temperature of 300ºC. The stress-strain relation is described in eq. (10), and the compressive strength and maximum strain of concrete are determined by eq. (13) ~ eq. (15).

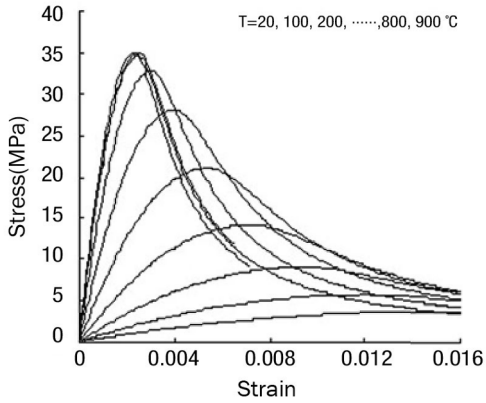

Fig. 5. Shi's Concrete Model [11]

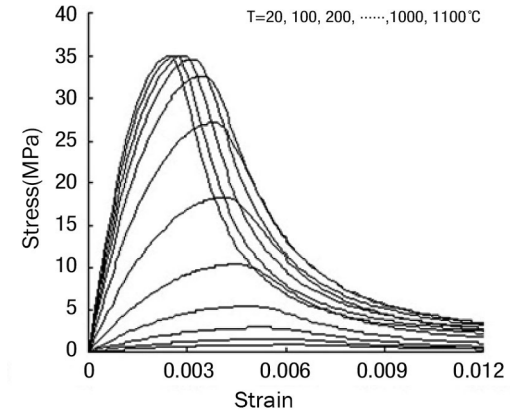

Fig. 6. Nan's Concrete Model [12]

$$y = 2x - x^2 (x \le 1) \quad (10a)$$

$$y = \frac{x}{5(x-1)^2 + x} (x > 1) \quad (10b)$$

$$y = \sigma / {f_c}^T \quad (11)$$

$$x = \varepsilon_\sigma / {\varepsilon_c}^T \quad (12)$$

$$\frac{f_c^T}{f_c} = \frac{1}{1+(0.17\gamma_T)^6} \quad (13)$$

$$\frac{\varepsilon_c^T}{\varepsilon_p} = 1 + (0.09 + 0.046\gamma_T)\gamma_T \quad (14)$$

$$\gamma_T = (T - 20)/1000 \quad (15)$$

$f_c$ : compressive strength of concrete at room temperature (MPa)
$f_c^T$ : compressive strength of concrete at TºC (MPa)
$\varepsilon_c^T$ : strain corresponding to $f_c^T$
$\varepsilon_c$ : strain corresponding to $f_c^T$
$\varepsilon_p$ : the maximum strain at room temperature (=0.0025)

The stress-strain curve of EUROCODE 2 [10] is presented in eq. (16) and Fig. 7, which is characterized by a parabolic increase and a linear decrease curve. The curve is described by eq. (16a) for strains less than or equal to $\varepsilon_{c1,\theta}$ and by eq. (16b) otherwise.

$$f = \frac{3\varepsilon f_{c,T}}{\varepsilon_{c1,T}\left(2+\left(\frac{\varepsilon}{\varepsilon_{c1,T}}\right)^3\right)}, \qquad \varepsilon \le \varepsilon_{c1,T} \quad (16a)$$

$f$ = straight decreasing line, $\varepsilon_{c1,T} < \varepsilon \le \varepsilon_{cu,T}$ (16b)
$f_{c,T}$ : compressive strength of concrete at TºC(MPa) (table 1)
$\varepsilon_{c1,T}$ : strain corresponding to $f_{c,T}$ (table 1)
$\varepsilon_{cu,T}$ : the maximum strain (table 1)

## 2.2 Steel Member

Many researchers have proposed temperature dependent stress-strain relations of a steel member as shown in Fig. 8, where the yield stress decreases rapidly according to the temperature increases. However, steel recovers its original yield strength when it cools to room temperature in a few studies [13].

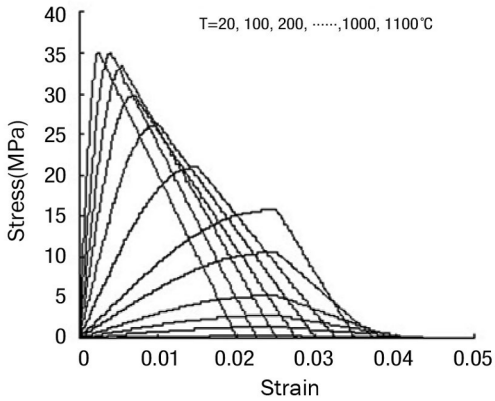


Fig. 7. Concrete Model in [10]

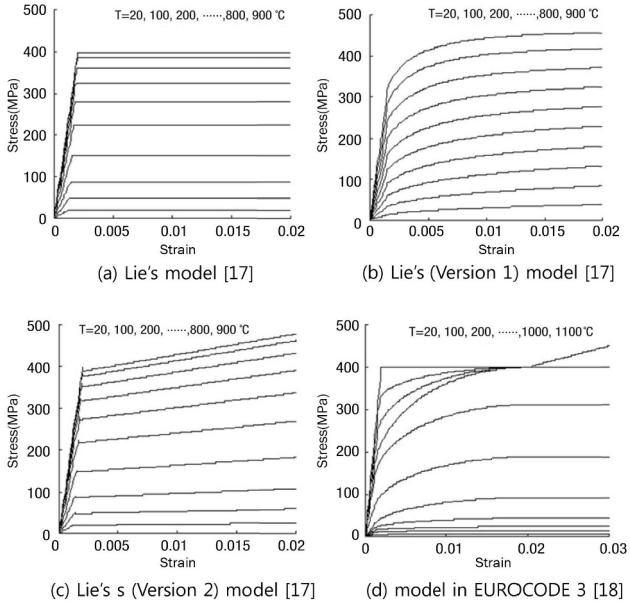


Fig. 8. Temperature Dependent Stress-strain Curves of a Steel Member

As described previously, steel rebar loses a significant part of its elastic modulus and yield strength during thermal loading but recovers almost all of them when it cools down to the ambient temperature. In this study, an embedded steel rebar recovered after a thermal loading experiment is used to measure the yield stress and tensile strength of the cooled rebar. For a parametric study, eight specimens including one that does not undergo thermal loading, another one without PP fiber (thermal loading) content, and a third one with 0.1% PP fiber (thermal loading) content were prepared for experiments. Measured yield stresses and tensile strengths of rebar are summarized in table 2, where almost all of the steel rebars, regardless of the thermal loading and PP fiber content, recovered to their original yield stresses and tensile strengths after cooling down. Therefore, it is concluded that the strength of a steel rebar drops significantly during thermal loading due to fire, but it recovers to its original strength after cooling down to room temperature.

# 3. FIRE EXPERIMENT AND THE RESULT

## 3.1 Test Specimen Setup

An RC slab specimen used in the fire loading and structural testing is shown in Fig. 9. This specimen describes the wall part of an underground box structure for a power supply. The thickness and rebar arrangement of the test specimen follow the actual specification of the box structure. The temperature sensors (K-type thermocouple) are located 20mm, 50mm (main rebar), 100mm, and 150mm (compressive rebar) from the fire exposed surface of the slab. Taking into consideration the construction errors of

**Table 2**. Yield Stress and Tensile Strength of Steel Rebar before Thermal Loading and after Cooling Down to Room Temperature.

| PP contents | yield load(kN) | max. load(kN) | yield stress (MPa) | tensile strength (MPa) |
|---|---|---|---|---|
| before fire 0 vol.% | 67.82 | 80.18 | 535.28 | 632.83 |
| | 68.42 | 82.10 | 540.02 | 647.99 |
| | 70.14 | 84.32 | 553.59 | 665.51 |
| after fire 0 vol.% | 67.90 | 81.92 | 535.91 | 646.57 |
| | 63.20 | 77.60 | 498.82 | 612.47 |
| after fire 0.1 vol.% | 68.04 | 82.64 | 537.02 | 652.25 |
| | 67.72 | 82.10 | 534.49 | 647.99 |
| | 66.84 | 81.30 | 527.55 | 641.67 |

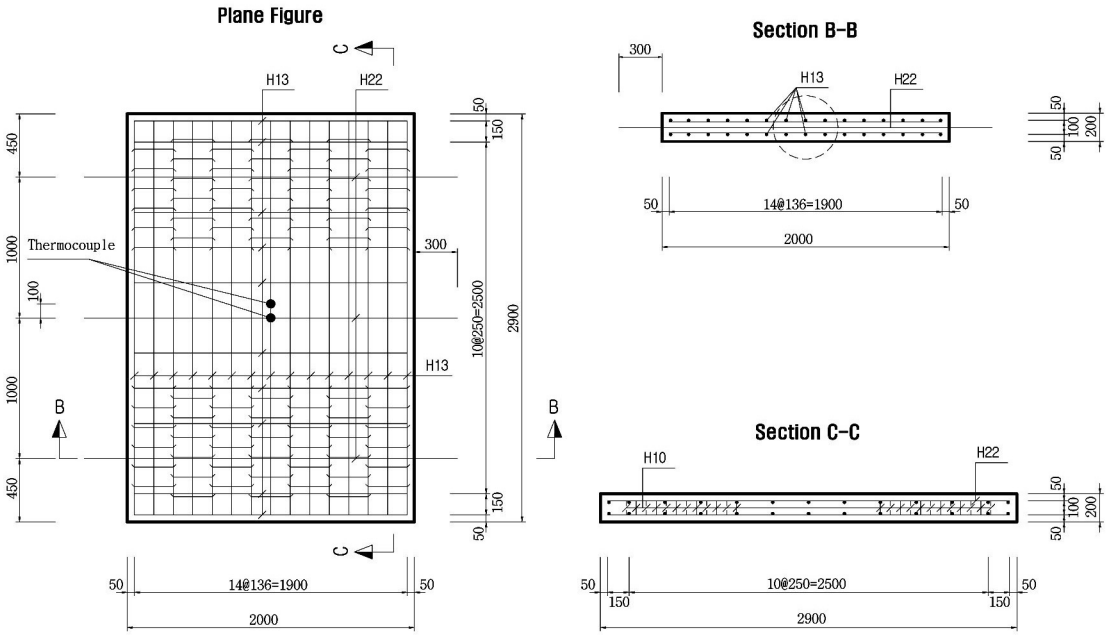


Fig. 9. Cross-section and Positions of Thermocouples to Measure Temperature

the specimen and the data collection errors of the fire test, the thermocouples were installed at two different places as shown in Fig. 9 (b). The specifications of the test specimen are listed in table 3. To prevent explosive spalling due to temperature increase, the percent of PP fiber in the test specimen was set to 0.10 vol.%.

### 3.2 Material Characteristic

The characteristics of the PP fiber in the test specimen are listed in table 4, and the mix proportions of concrete with 35MPa design strength are shown in table 5. A cylindrical standard specimen has an average of 30MPa 28-day strength due to air curing.

### 3.3 Standard Fire Test using ISO 834.

The ISO 834 curve ([19], [20]), specified mainly for building structures, is widely applied in standard fire-resistance tests as a temperature condition. The ISO 834 fire curve is determined by eq. (17).

$$T(t) = 345 \cdot log(8t + 1) + T_a \quad (17)$$

$t$ : fire exposure time (min)
$T(t)$ : temperature at time $t$ (ºC)
$T_a$ : ambient temperature (20ºC)

The fire-resistance test is the thermal loading of an ISO 834 fire curve on one surface of a specimen for 180 minutes. The shape of furnace and the specimen after the test are shown in Figs. 10(a) and 10(b).

### 3.4 Results of ISO 834 Fire Test.

The surface condition of the thermally loaded concrete is shown in Fig. 11. The general specimen without PP fiber exhibited damage due to a small explosion, whereas the specimen with 0.1vol.%. PP fiber showed no sign of popping expansion damage. The thickness at which the slab separated due to the spalling varied from point to point.

The time history of temperature measured inside the test specimens is presented in Fig. 12. In the case of the general specimen without PP fiber content in Fig. 12(a), the temperature at a depth of 20mm was very similar to that of the thermal loading temperature because some of the concrete separated during the thermal loading due to explosive spalling. As depth increased, the temperature dropped and converged at depths over 150mm. In the case of the specimen with PP fiber contents shown in Fig. 12(b), the temperature dropped significantly even at a depth of 20mm because the concrete had no separation due to a spalling.

Fig. 13 presents measured temperatures according to the position from the surface of the concrete at specific times during the thermal loading. Temperature decreases up to a depth of 150mm and converges afterwards. The specimen with PP fiber contents showed temperature variations up to a depth of 100mm but converged afterwards.

KS (Korea Standard) F 2257-7[21] specifies that the average temperature of rebar in columns and beams should be 538ºC and that it should be less than 649ºC under the ISO 834 fire test. After 120 minutes of fire attack, a rebar close to the surface of the specimen without PP fiber contents violated this specification, whereas the temperature of the rebar in the specimen with PP fiber contents remained below the KS F 2257-7 specification (Table 6).

**Table 3**. Types of Test Specimen

| PP ratio (vol.%) | No. of specimens | remark |
|---|---|---|
| 0 | 2 | 1 for extra test |
| 0.10 | 1 | |

**Table 4**. Properties of PP Fibers

| | Polypropylene fibers |
|---|---|
| Density ($g/cm^3$) | 0.91 |
| Diameter ($\mu m$) | 21.6~39.4 |
| Length ($mm$) | 5~10 |
| Tensile strength ($MPa$) | 328.3~367.7 |
| Elastic modulus ($GPa$) | 3.0~3.2 |

(a) Shape of furnace (b) Specimen after fire test

Fig. 10. Procedure of Fire Test

(a) The general specimen (b) The specimen with PP fiber(0.1 vol.%)

Fig. 11. The Surface Condition of Thermally Loaded Concrete

**Table 5**. Mix Proportions of Concrete with 35MPa Design Strength ($kg/m^3$)

| W/C (%) | S/a(%) | Water | Cement | Sand | Gravel | Admixture | PP fibers |
|---|---|---|---|---|---|---|---|
| 38.5 | 38.9 | 170 | 442 | 692 | 1113 | 3.49 | 0.0~0.91 |

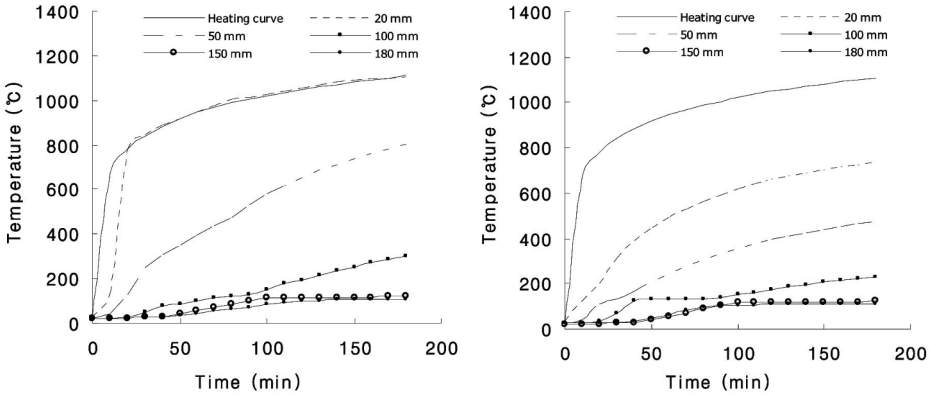


(a) PP fiber contents: 0.0 vol.% (b) PP fiber contents : 0.1 vol.%

Fig. 12. Temperature Evolution of Slabs

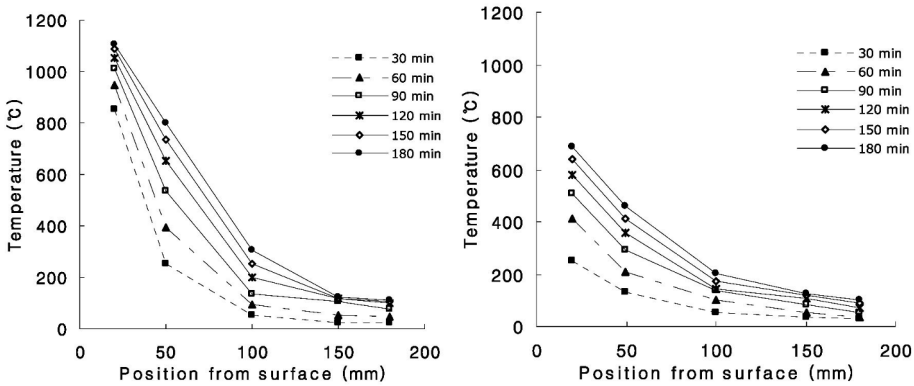


(a) PP fiber contents: 0.0 vol.% (b) PP fiber contents : 0.10 vol.%

Fig. 13. Temperature at the Thermocouple Positions

**Table 6**. Temperature of Steel Rebar (°C)

| PP fiber contents (vol.%) | Steel rebar | Depth from surface (mm) | Heating duration(min) | | |
|---|---|---|---|---|---|
| | | | 60 | 120 | 180 |
| 0.0 | C2 | 50 | 396.0 | 655.8 | 802.7 |
| | C4 | 150 | 55.0 | 116.1 | 124.4 |
| 0.10 | C2 | 50 | 211.3 | 359.8 | 456.9 |
| | C4 | 150 | 53.2 | 108.2 | 123.3 |

## 4. STRUCTURAL TEST AFTER FIRE TEST AND COOLING DOWN

### 4.1 Structural Loading Test Setup

The specimens used in the ISO 834 fire test were cooled down to room temperature and the structural loading test followed. To yield bending failure, the edges of the RC slab were simply supported and the remaining strength of the structure was evaluated after the fire damage. A 1000kN actuator was used to produce and measure the deflection at the center. The test setup is shown in Fig. 14.

Fig. 14. Structural Test Setup after ISO 834 Fire Test

### 4.2 Results of Structural Loading Test

The load-deflection curve from the structural load test is shown in Fig. 15. The maximum resistant load of the specimen without PP fiber content was 253.8kN, which was about 80% of that of the specimen with PP fiber content (316.9kN). Furthermore, although both specimens showed similar ductile behavior, the stiffness and maximum strength of the specimen without PP fiber content were significantly lower than those of the specimen with PP fiber content. This difference is due to the explosive separation of concrete following the increase in temperature.

## 5. STRUCTUAL ANALYSIS OF THE FIRE TEST SPECIMEN

### 5.1 Temperature Dependent Material Model

The stress-strain relation of the concrete specimen used in the fire test was determined from the curve of the measured temperature versus depth of the cross section, and nonlinear structural analyses were performed using this relationship. The mechanical characteristics of concrete cannot recover from damage due to temperature increase. It is generally assumed that the stress-strain relation of concrete after cooling down is similar to that of the heated (damaged) concrete. The material characteristics of a steel rebar are affected by the temperature increase significantly, but a rebar recovers its original strength after the cooling process [21]. In this analysis, an elastic-perfect plastic model at room temperature (20ºC) is chosen among the temperature dependent steel models suggested by Lie [17]. A general purpose finite element program 'Abaqus' with 'Concrete' model was utilized for analysis [23].

Temperature dependent stress-strain curves of concrete from the references are all different from one another and they are compared and investigated. The maximum temperatures measured versus the cross section concrete depth during a fire test is summarized in table 7.

In the case of specimens without PP fiber content, the formula of Schneider [15] showed decreasing material performance up to 150mm depth, whereas the formula from EUROCODE 2 [10] showed the convergence of material performance around 100mm depth. The Lie [7] formula showed weakening material up to 100mm depth, whereas the Shi et al [11] and Nan et al [12] formulae showed convergence of the material strength at around 50mm depth. In the case of specimens with PP fiber content, overall performance near the surface of thermal loading was enhanced. Figures (Fig. 16 - Fig. 20) present various material models.

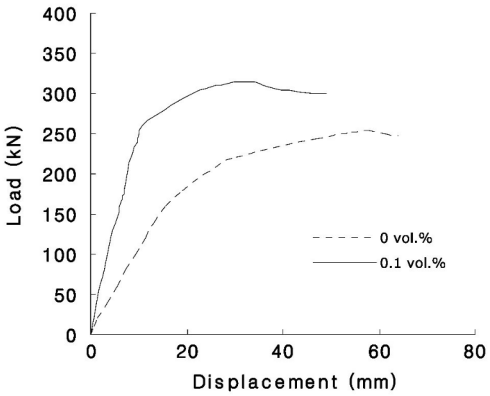

Fig. 15. Load-deflection Curve

**Table 7**. Maximum Temperature Versus Depth of the Concrete Cross Section

| distance from the heating surface (mm) | Max. temperature (°C) | |
|---|---|---|
| | without PP fiber | with PP fiber |
| 0 (surface) | 1117.74 | 1117.74 |
| 20 | 1108.1 | 685.9 |
| 50 | 802.7 | 456.9 |
| 100 | 304.5 | 205.5 |
| 150 | 124.4 | 123.3 |
| 180 | 111.1 | 99.5 |
| opposite surface | 80.1 | 79.5 |

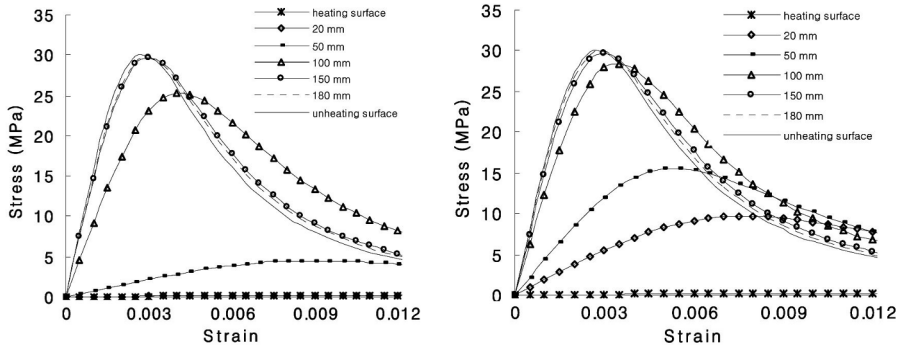

(a) PP fiber contents: 0.0 vol.% (b) PP fiber contents : 0.10 vol.%

Fig. 16. Stress-strain Relation after Fire Test [15]

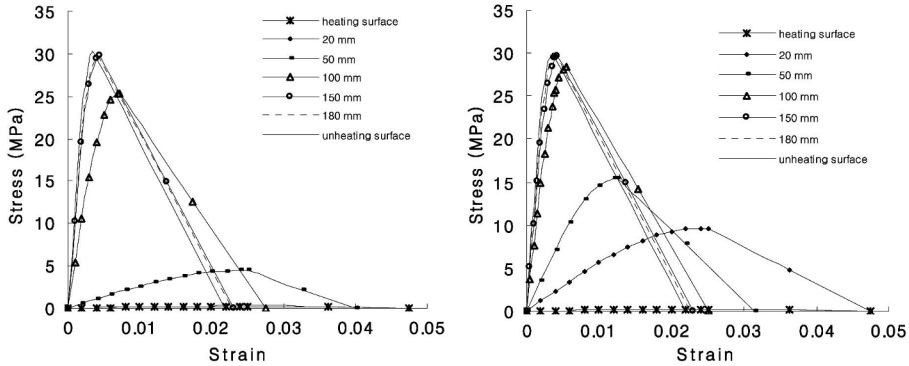


Fig. 17. Stress-strain Relation after Fire Test [10]

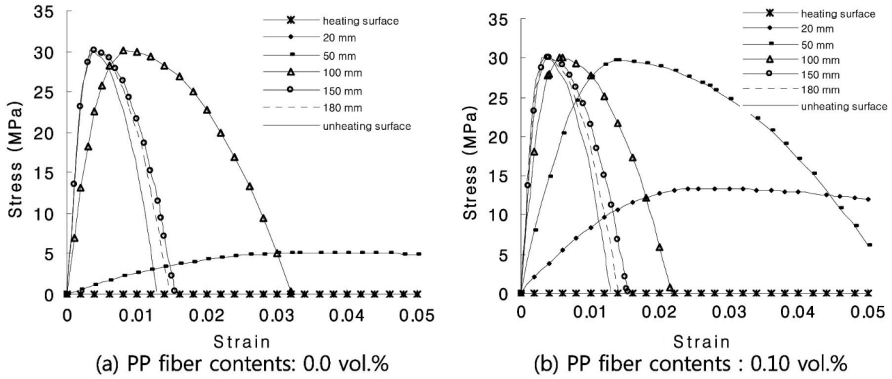


Fig. 18. Stress-strain Relation after Fire Test [7]

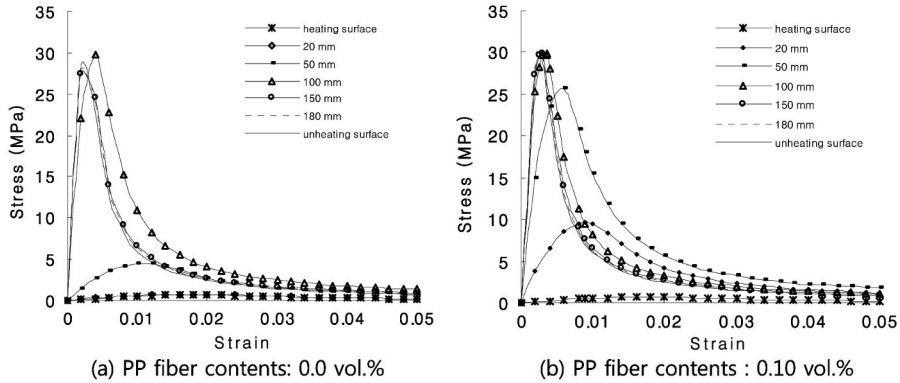


Fig. 19. Stress-strain Relation after Fire Test [11]

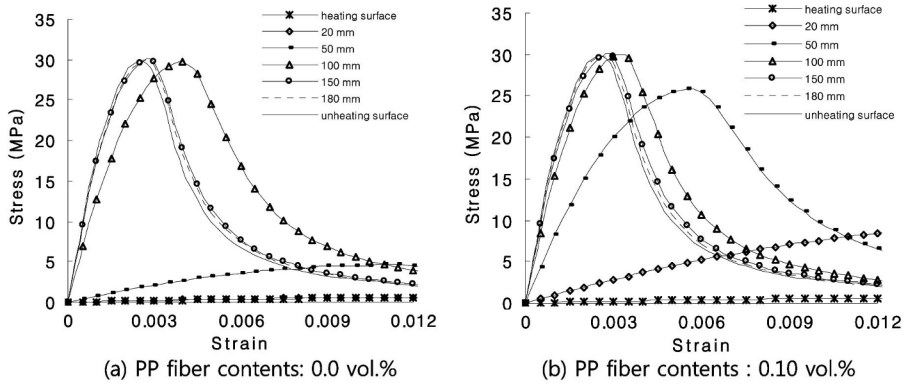


Fig. 20. Stress-strain Relation after Fire Test [12]

Temperature dependent stress-strain relations for each depth are presented in Fig. 21 and Fig. 22 according to the above mentioned formulae. Fig. 21 shows the case of concrete with 0% PP fiber content: the strength is very small up to 50mm depth and the strains at the maximum calculated stresses show large differences. Fig. 22 presents the case of concrete with 0.1vol.% PP fiber content: a good portion of the strength is maintained within the 50mm depth

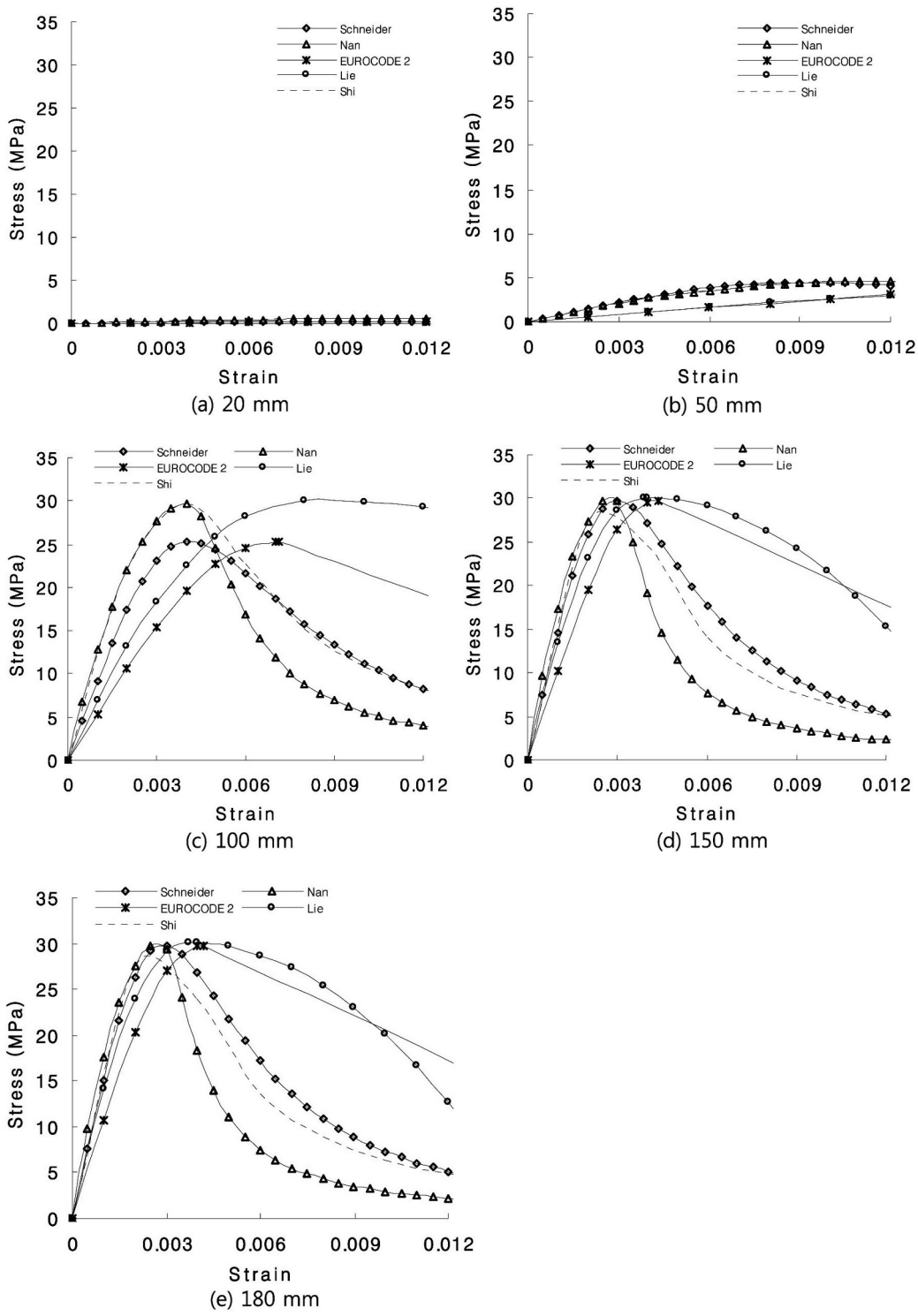


Fig. 21. Stress-strain Relation of Concrete for Each Depth (PP Fiber Content: 0 vol.%)

area. The strength of the concrete does not vary much for each formula, whereas the magnitude of strain varies at 100mm depth.

## 5.2 Structural Analysis after Cooling Down

Using the stress-strain relations presented in the previous section, the resistances of the cross section after fire

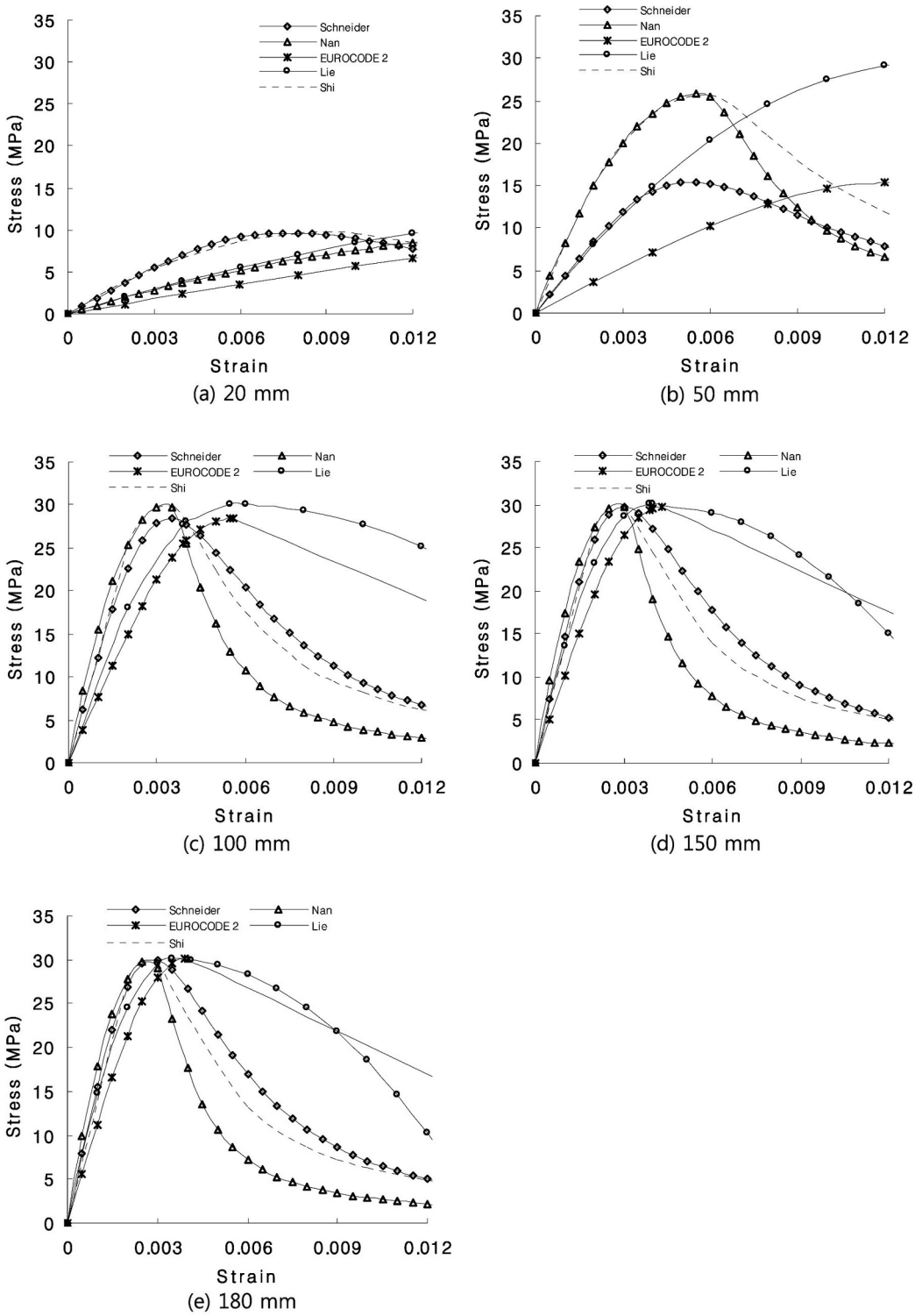


Fig. 22. Stress-strain Relation of Concrete for Each Depth (PP Fiber Content: 0.10 vol.%)

damage were evaluated by nonlinear finite element analysis. In the stress-strain relations of concrete, the maximum temperature during the fire test was applied according to Fig. 23. The strength reduction of the steel was not considered, and an elastic-perfect plasticity model [7] was applied to all analyses.

### 5.3 Result Analysis

The maximum resistances of all cases are listed in Table 8. The results in Fig. 24 present the case of the specimen without PP fiber content. The Lie model [7] yielded curves which matched well with the test results. The result using EUROCODE2 [10] showed some differences of the stiffness near the initial stage. The difference of the maximum resistance was about 5.8%. The Schneider [15] model and Nan et al. [12] models matched the test results well, whereas the Shi et al [12] model estimated the resistance of the cross section to be about 19% lower than that of the actual test.

The results in Fig. 25 present the case of the specimen with 0.1% PP fiber content. The Lie [7] model and Nan et al [12] model closely estimated the test results at about 101~103%, whereas the EUROCODE 2 [10] model and Schneider [15] model underestimated the results at about 91~95%. Table 11 shows that the measured resistance load of the 0.1vol.% PP specimen during the test increased by about 24% from that of the 0 vol.% case. In the analysis, the resistance load of each model increased by 107~155% compared to the non-PP fiber case, and the Lie model most closely matched the actual resistance load level.

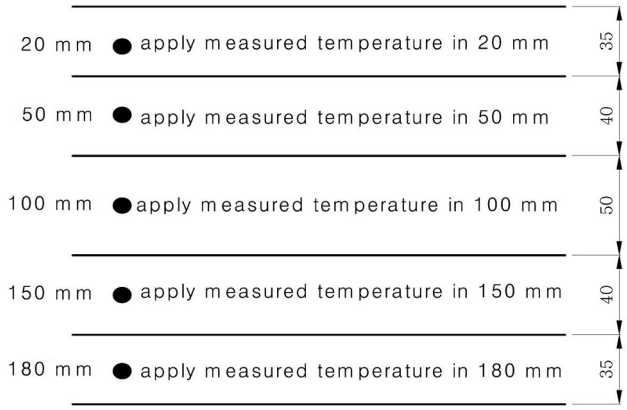


Fig. 23. Stress-strain Application Range for Each Temperature

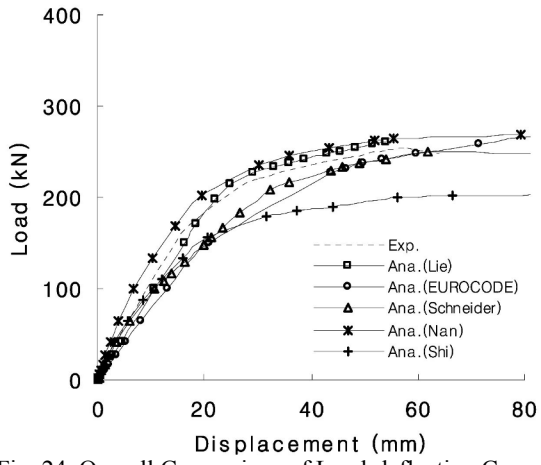


Fig. 24. Overall Comparison of Load-deflection Curves (PP Fiber Contents : 0 vol.%)

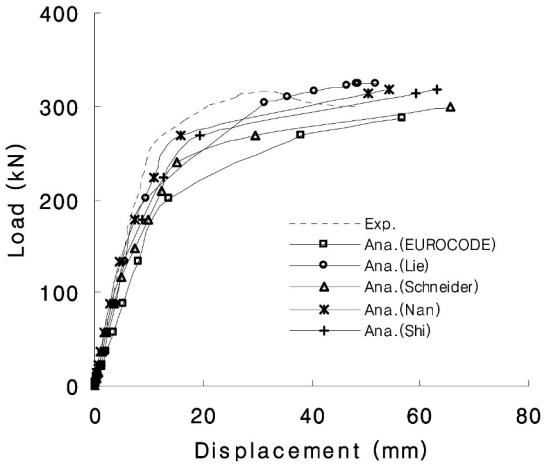


Fig. 25. Overall Comparison of Load-deflection Curves (PP Fiber Content: 0.1vol.%)

**Table 8**. Maximum Resistance (Test and Analysis Result)

| Max. resistance measuring condition | | Depth from surface (mm) | |
|---|---|---|---|
| | | PP fiber 0.vol.% | PP fiber 0.1vol.% |
| Test result | | 253.8 | 316.9 |
| Analysis result | Lie model [7] | 260.1 | 324.0 |
| | EUROCODE 2 model [10] | 268.5 | 286.4 |
| | Schneider model [15] | 249.6 | 299.6 |
| | Nan et al model [12] | 269.7 | 317.6 |
| | Shi et al model [11] | 205.5 | 317.6 |

## 6. CONCLUSIONS

In this study, the temperatures of an RC slab at each depth are measured during a fire experiment (thermal loading test) based on the ISO 834 fire curve. The remaining strength of the structure after the thermal loading is evaluated at room temperature. Applications of the temperature curve obtained from the thermal test to the stress-strain curves from many previous studies are investigated. Nonlinear finite element analyses using the stress-strain-temperature relation are performed and the following conclusions are made:

1. An explosive spalling was witnessed during the fire experiment for the specimen without PP fiber, but not for the specimen with PP fiber. The thickness at which the slab separated due to the spalling varied from point to point.
2. In the case of the specimen without PP fiber, the temperature at a depth of 20mm was very close to that of the thermal loading itself because the concrete surface was separated due to spalling, whereas in the case of the specimen with PP fiber, temperature decreased significantly at a depth of 20mm because the concrete surface had no damage. Regardless of the type of specimen, temperature decreased up to a depth of 150mm and showed no significant change afterwards.
3. Measured temperatures during the fire experiment were applied to the models of Schneider, EUROCODE 2, Lie, Shi et al, and Nan et al, where the stress-strain relationship for each depth was set accordingly. The strengths of the specimen without PP fiber predicted by the various models were very low up to a depth of 50mm and they were similar at a depth of 100mm, whereas the corresponding strains were quite different depending on the model used. The strengths of the specimen with PP fiber were maintained relatively well within a depth of 50mm and they were similar at 100mm depth. The overall performance of the specimen with PP fiber was enhanced near the surface of thermal loading.
4. The ultimate strengths of real specimens were compared with analytic results obtained from the various concrete stress-strain-temperature models. For the specimen without PP fiber, Lie's model gave results that were the closest to the test results. The stiffness predicted by the EUROCODE 2 model was different from the test result and it underestimated the strength by about 5.8%. The Schneider model and Nan et al model predicted the test results well, whereas the Shi et al model underestimated the strength at about 81%. For the specimen with PP fiber, the EUROCODE 2 model and Schneider model underestimated the strength at about 91% and 95%, respectively, whereas the other models gave relatively accurate estimations at about 101-103%.
5. The test result showed that the addition of 0.1vol.% PP fiber enhanced the strength of the specimen up to 124%. The analyses using several material models estimated 107% to 155% strength enhancement, whereas the Lie model estimated the actual strength enhancement the closest at 125%.

## ACKNOWLEDGEMENT

The present study was conducted by the research fund of Dankook University in 2011.

## REFERENCES

[1] A. Nishida, N. Ymazaki, H. Inoue, U. Schneider, and U. Diederichs, "Study on the properties of high-strength concrete with short polypropylene fibre for spalling resistance." *Proceedings of International Conference on Concrete under Severe Conditions*, CONSEC'95, Vol. 2, Sapporo, Japan, pp.1141-1150 (1995).

[2] T. Atkinson, "Polypropylene fibers control explosive spalling in high- performance concrete." Concrete, Vol. 38, No. 10, pp.69-70 (2004).

[3] J. A. Purkiss, "Steel fibre reinforced concrete at elevated temperatures." *International Journal of Cement Composites and Light weight Concrete*, Vol. 6, No.3, pp.179-184 (1984).

[4] T. T. Lie and V. K. R. Kodur, "Thermal and mechanical properties of steel-fibre-reinforced concrete at elevated temperatures."*Canadian Journal of Civil Engineering*, Vol. 23, pp.511-517(1996).

[5] S. L. Suhaendi and T. Horiguchi, "Effect of short fibers on residual permeability and mechanical properties of hybrid fibre reinforced high strength concrete after heat exposition." *Cement and Concrete Research*, Vol. 36, pp.1672-1678 (2006).

[6] H. Y. Kim, H. S. Chea, H. K. Jeon, and K. S. Youm "Proposal for the model and properties of compressive strength at high temperature for the high strength concrete mixed with fiber cocktail." *Proceedings of the Korea Concrete Institute*, Vol. 19, No. 9, pp.605-608 (2007).

[7] T. T. Lie,Structural fire protection : *Manual of practice*, New York: American Society of Civil Engineers, pp.199-201 (1995).

[8] W. Ritter, "Die bauweisehennebique." (In German), *SchweizerischeBauzeitung*, Vol. 33 (1899).

[9] E. Hognestad, "A study of combined bending and axial load in reinforced concrete members." *Bulletin* No.399, University of Illinois Engineering Experiment Station, Urbana, IL (1951).

[10] EUROCODE 2, *Design of concrete structures-Part 1.2: General rules- stuructural fire design*, Commission of the European Communities, Brussels, Belgium (2004).

[11] X. Shi, T. H. Tan, H. T. Kang and Z. Guo, "Concrete constitutive relationships under different stress-temperature paths." *Journal of Structural Engineering*, December 2002, pp.1511-1518 (2002).

[12] J. Nan, Z. Guo and X. Shi"Thermo-mechanical coupling constitutive relationship of concrete at high temperature." *Proceedings of the 2nd International Congress*, June 5-8, 2006-Naples, Italy Session12 - Response of concrete structures to high temperatures and fire (2006).

[13] J. Outinen and P. Makelainen "Mechanical properties of structural steel at elevated temperatures and after cooling

down." *Proceeding of the second international workshop, Structures in Fire, SiF 02'*, pp.273-289 (2002).
[14] U. Schneider and A. Haksever, *Bestimmung der aquialenten branddauer von statisch bestimmt gelagerten stahlbetonbalken bei naturlichen branden*, (In german), Bericht des Instituts fur Baustoffkunde und Stahlbetonbau der Technischen Universitat Braunschweig (1976).
[15] U. Schneider, "Concrete at high temperatures-a general review." *Fire Safety Journal*, 13, pp.55-68 (1988).
[16] J. M. Franssen, "Plastic analysis of concrete structures subjected to fire." *Proc. of the Workshop on Fire Design of Concrete Structures*, Milano, Italy, December (2004).
[17] T. T. Lie, S*tructural fire protection*, New york: American Society of Civil Engineers (1992).
[18] EUROCODE 3, *Design of steel structures, Part 1.2, structural fire design*, Commission of the European Communities, Brussels, Belgium (1995).
[19] ISO, *Fire resistance tests-elements of building construction, International Standard ISO 834*, Geneva (1975).
[20] H. Yang, L. H. Han and Y. H. Wang, "Effects of heating loading histories on post-fire cooling behaviour of concrete-filled steel tubular columns." *Journal of Constructional Steel Research*, 64, pp.556-570 (2008).
[21] KS, Korean Industrial Standards, *Methods of fire resistance test for elements of building construction-Specific requirements for columns*, KS F 2257-7, Korean Standards Association (2005).
[22] C.-H. Chung, C.-R. Im, H.-J. Kim and S.-H. Joo, "Evaluation of Fire Performance oc RC Slabs with Half-Depth Precast Panels." *Journal of the Korean Society of Civil Engineers*, Vol. 30, No.4A (2010).
[23] Abaqus, *Analysis User's Manual*, version 6.8 (2008).